Article

Nanofiber Configuration of Electrospun Scaffolds Dictating Cell Behaviors and Cell-scaffold Interactions

LI Haiyan[1], LIU Mingyue[1], WANG Xiaoyu[1], WANG Hongsheng[1], MO Xiumei[1] and WU Jinglei[1,2]✉

Received January 16, 2021
Accepted March 6, 2021

Electrospun nanofibers are of the same length scale as the native extracellular matrix and have been extensively reported to facilitate adhesion and proliferation of cells and to promote tissue repair and regeneration. With a primary focus on tissue repair and regeneration using electrospun scaffolds, only a few studies involved electrospun nanofiber scaffolds directing cell behaviors have been reported. In this study, we prepared electrospun nanofiber scaffolds with distinct fiber configurations, namely, random and aligned orientations of nanofibers, as well as oriented yarns, and investigated their effects on cell behaviors. Our results showed that these scaffolds supported good proliferation and viability of murine fibroblasts. Fiber configuration profoundly influenced cell morphology and orientation but showed no effects on cell proliferation rate. The yarn scaffold had comparable total protein accumulation with the random and aligned scaffolds, but it supported a greater proliferation rate of fibroblasts with significantly elevated collagen deposition due to its porous fibrous configuration. Cell-seeded yarn scaffolds showed a greater Young's modulus compared with cell-free controls as early as 1 week. Together with its unique fiber configuration similar to the native extracellular matrix of the myocardium, the yarn scaffold might be a suitable matrix material for modeling cardiac fibrotic disorders.

Keywords Electrospinning; Nanofiber configuration; Fibroblast; Cell proliferation; Biomechanics

1 Introduction

Electrospun nanofibers show similarity in length scale with the native extracellular matrix and are beneficial to cell adhesion and proliferation [1]. This feature makes electrospun nanofibers good candidates for scaffolding materials in many tissue engineering and regenerative medicine applications[2]. In addition to the unprecedented superiority for cell growth, electrospun nanofibers could also regulate cell behaviors through special fiber configurations, such as fiber orientation and porosity[3,4]. For instance, aligned nanofibers dictate cells into an elongated shape and growing along the fiber direction[5,6]. This indicates that electrospun nanofiber scaffolds might be good candidates for cell culture matrix to investigate cell-material interactions and to model disease milieus. Collagen is the most abundant extracellular matrix component throughout the body[7]. Fibroblast is the master cell producing collagen, which is dynamically regulated by various cells, growth factors, and enzymes[8,9]. On the one hand, collagen deficiency delays healing processes and results in inferior tissue regeneration during wound healing. On the other hand, abnormally elevated deposition and increased crosslinking of collagen give to scar formation, which is fatal in some circumstances, such as myocardial and pulmonary fibrosis[9,10]. While current research on the cellular biology of fibroblast largely relies on the conventional culture of those cells on polystyrene tissue culture plates. Despite the unmet need, there is no well-established platform for culturing fibroblasts in a three-dimensional manner that mimics the native microenvironment where fibroblasts reside[5,8,10,11].

Previously, we have reported an electrospinning technique, by which as-electrospun nanofibers are twisted into yarn bundles in a dynamic liquid system[12,13]. This yarn scaffold has an aligned nanofibrous structure mimicking the three-dimensional of the native extracellular matrics of many tissues. It allows cells to grow in a three-dimensional pattern with an aligned organization[14,15]. We hypothesized that this yarn scaffold can serve as a three-dimensional niche for fibroblast growth to model fibroblast-associated disorders. To verify our hypothesis, we prepared electrospun scaffolds with distinct fibrous textures and assessed their interactions with murine fibroblasts in terms of viability, proliferation, and morphology, as well as the effects of fibroblast-secreted extracellular matrix on the mechanical properties of fibroblast-seeded scaffolds.

2 Experimental

2.1 Preparation and Characterization of Electrospun Scaffolds

2.1.1 Materials

Poly(lactide-co-caprolactone)(PLLA-CL, LA:CL=75:25, molar

✉ WU Jinglei
jw@dhu.edu.cn
1. Key Laboratory of Science and Technology of Eco-Textile, Ministry of Education, College of Chemistry, Chemical Engineering and Biotechnology, Donghua University, Shanghai 201620, P. R. China;
2. Department of Plastic and Reconstructive Surgery, Shanghai Key Laboratory of Tissue Engineering, Shanghai Ninth People's Hospital, School of Medicine, Shanghai Jiao Tong University, Shanghai 200011, P. R. China

ratio) was provided by Jinan Daigang Biomaterial Co., Ltd.(Jinan, China). 1,1,1,3,3,3-Hexafluoro-2-propanol(HFIP) was purchased from Da-Rui Fine Chemical Co., Ltd.(Shanghai, China). Type A gelatin derived from porcine skin(*ca*. 300 g Bloom) was provided by Sigma-Aldrich.

2.1.2 Scaffold Preparation

Electrospun scaffolds with distinct fibrous orientations and configurations were prepared following our previous reports[16,17]. PLLA-CL and gelatin were dissolved in HFIP at the concentration of 12%(g/mL) with a PLLA-CL/gelatin ratio of 8:2(mass ratio). The PLLA-CL/gelatin solution was fed at 1 mL/h and charged with a high voltage of 15 kV to generate nanofibers. The as-electrospun nanofibers were collected by a slow-speed mandrel(8 cm in diameter, 90 r/min) or a high-speed mandrel (10 cm in diameter, 3000 r/min) at a distance of 10 cm to obtain randomly oriented nanofiber membranes or aligned nanofiber membranes, respectively. To obtain yarn scaffold, the as-electrospun nanofibers were deposited in a dynamic liquid tank to form yarns that were then collected by a slow-speed mandrel(5 cm in diameter, 90 r/min) to form yarn membranes[12].

2.1.3 Scaffold Characterization

The scaffold morphology was visualized by mens of scanning electron microscopy(SEM). Samples were mounted on a conductive tape and sputter-coated with gold and observed under a scanning electron microscope(Phenom XL Desktop, Phenom, Netherlands) at an accelerating voltage of 5 kV.

Tensile properties of electrospun membranes were determined in the wet state. Samples were tailored into strips(10 mm×40 mm) and incubated in phosphate-buffered saline(PBS) at 37 °C for 24 h prior to the uniaxial tensile test. For aligned and yarn scaffolds, samples were tailored along the direction of fiber alignment. Specimens were clamped by the grips of a universal testing machine(Instron 5567, Norwood, MA) with a 200 N load cell and stretched at a crosshead speed of 5 mm/min until failure. Ultimate tensile strength(UTS) and strain at failure were obtained from the stress-strain curves at the points of maximum tensile strength. Young's modulus was calculated as the slope of the initial 5% linear portion from the stress-strain curve(n=4).

2.2 Cell Growth on Electrospun Scaffolds

2.2.1 Cell Seeding

NIH 3T3 murine fibroblasts were obtained from the Cell Bank of the Chinese Academy of Science. Fibroblasts were maintained and expanded in a high glucose Dulbecco's modified Eagle medium(Hyclone) supplemented with 10% fetal bovine serum(Gibco) and 1% penicillin/streptomycin. Cells at 80% confluence were trypsinized and centrifuged for seeding with electrospun scaffolds.

Electrospun membranes were punched to disc scaffolds with appropriate sizes to fit 48 well plates(11 mm in diameter) and 12 well plates(22 mm in diameter). Scaffolds were disinfected with 70% ethanol for 1 h followed by UV irradiation overnight. Before cell seeding, scaffolds were prewetted with a complete medium. Cells were seeded onto the surface of scaffolds at a density of 2×10^4 cells/cm^2. Cell-seeded scaffolds were placed in a 37 °C incubator with 95% humidity and 5% CO_2. The medium was refreshed every other day.

2.2.2 Cell Proliferation

The proliferation rate of the cells cultured on scaffolds was determined by Cell Counting Kit-8(CCK-8, Beyotime Biotechnology, Shanghai, China) assay following the manufacturer's instructions. Cell-seeded scaffolds were incubated with CCK-8 for 1.5 h at 37 °C, and then 100 μL of supernatant of each well was read at 450 nm using a plate reader(Multiskan MK3, Thermo, USA). CCK-8 assay was performed at days 1, 4, and 7(n=4).

2.2.3 Cell Viability

Cell viability was evaluated by live/dead staining. At days 1, 4, and 7, cell-seeded scaffolds were rinsed with PBS followed by incubating with calcein-AM and propidium iodide(Beyotime Biotechnology, Shanghai, China) for 30 min at 37 °C, then briefly washed with PBS and visualized by a fluorescence microscope(DMi 8, Leica, Germany)(n=3).

2.2.4 Cell Morphology

Cell morphology was observed under an SEM. At days 1, 4, and 7, cell-seeded scaffolds were harvested and fixed in 4% paraformaldehyde and freeze-dried. Samples were then sputter-coated with gold and visualized under an SEM.

2.3 Cell-scaffold Interactions

2.3.1 Biomechanics of Cell-seeded Scaffolds

Tensile properties of cell-seeded scaffolds(22 mm diameter) were determined 1, 2, and 3 weeks after cell seeding. Samples were tailored into strips(5 mm×20 mm, along the direction of fiber alignment if applicable) and tested as the aforementioned

https://doi.org/10.1007/s40242-021-1024-7

method(n=4). Cell-free scaffolds incubated under the same condition were served as controls for comparing with their corresponding cell-seeded scaffolds(n=4).

2.3.2 Collagen Deposition

Collagen contents of cell-seeded scaffolds were determined by a hydroxyproline assay. After the biomechanical test, samples were collected and stored at –20 °C until hydroxyproline assay. Samples were hydrolyzed within 3 mol/L sulfuric acid at 105 °C for 2 h. Hydrolysate solution was incubated with equal chloramine T solution for 20 min at room temperature. Then color reagent was added to the mixture and incubated at 65 °C for 20 min. The absorbance of the solution was read at 558 nm using a plate reader(n=4). The concentration of hydroxyproline was calculated against a standard curve with known concentrations of hydroxyproline. Deposited collagen content on each scaffold was calculated from hydroxyproline using a converting factor of 7(n=4).

2.3.3 Total Protein Accumulation

At weeks 1, 2, and 3, cell-seeded scaffolds were harvested and lysed by cell lysis buffer(Beyotime Biotechnology, Shanghai, China) and stored at –20 °C until analysis. Prior to assay, samples were thawed at room temperature and centrifuged at 13000 r/min for 5 min at 4 °C. Supernatants were then incubated with BCA solution(Beyotime Biotechnology, Shanghai, China) for 30 min at 37 °C. The absorbance of incubation was read at 562 nm using a Multiskan MK3 plate reader(n=5). A standard curve of known concentrations of bovine serum albumin was made to calculate the amounts of total proteins.

2.4 Statistical Analysis

Data were presented as means±standard deviations. Statistical analyses were performed by one-way or two-way ANOVA followed by Tukey's post hoc test or Student's t-test where appropriate. Statistical significance was considered at p<0.05.

3 Results and Discussion

3.1 Scaffold Properties

Manipulation of electrospun nanofibers through different collecting systems allows nanofiber scaffolds with distinct configurations, which profoundly influences their biological performance[2,4]. Conventional electrospinning techniques that deposit nanofibers on a flat collector give to randomly oriented nanofibers that configure into a dense membrane[Fig.1(A)]. This random nanofiber membrane showed dense nanofiber configuration with an interfiber distance of less than 10 μm. Nanofibers were collected *via* a high-speed mandrel, by which nanofibers were dragged into a highly organized manner with nanofibers well aligned along the circumferential direction of

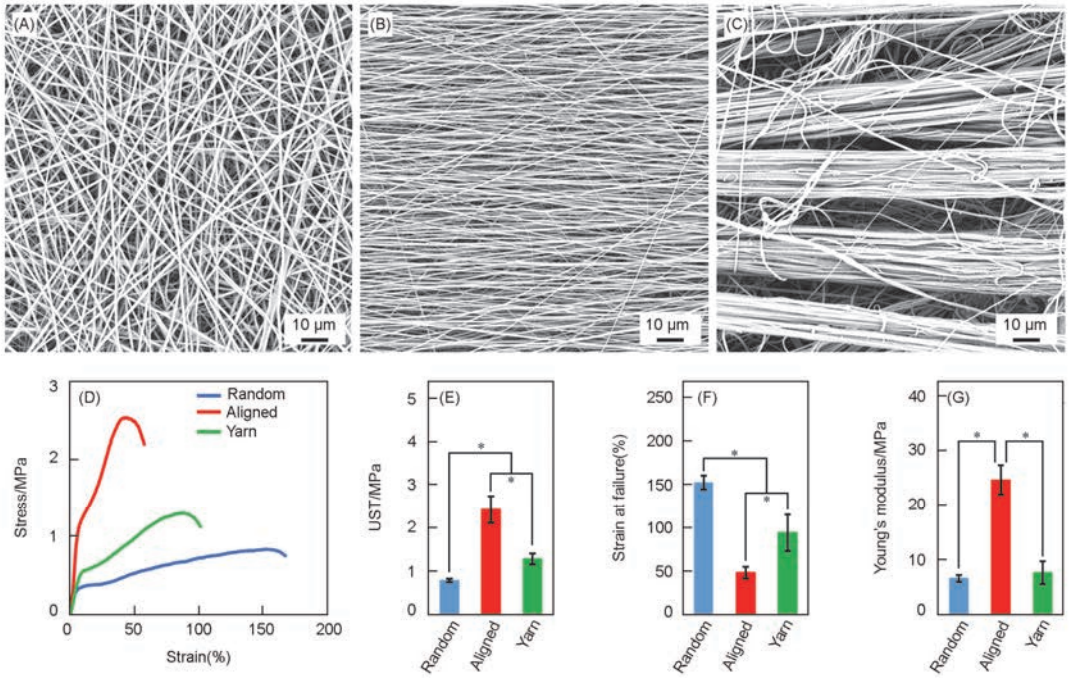

Fig.1 SEM images of the random(A), aligned(B), and yarn(C) scaffolds, representative stress-strain curves(D) with UTS(E), strain at failure(F), and Young's modulus(G) of electrospun scaffolds

Note: tensile strengths of aligned and yarn scaffolds are tested along the direction of fiber alignment. One-way ANOVA, * indicates p<0.05.

https://doi.org/10.1007/s40242-021-1024-7

the rotating mandrel[Fig.1(B)]. The aligned nanofiber membrane also showed a dense fiber configuration with an even smaller interfiber distance of less than 3—5 μm. Recently, we have reported a dynamic liquid system for electrospinning, by which nanofibers are twisted into yarn bundles and subsequently manipulated into a porous membrane[12,16]. The yarn scaffold was mainly composed of aligned yarns with diameters of approximately 20—30 μm[Fig.1(C)]. The yarns had a rough surface texture with a visible nanofiber configuration and showed a greater inter yarn distance of approximately 10—20 μm. In this study, we selected PLLA-CL and porcine skin-derived gelatin for fabricating electrospun scaffolds because we and other groups have proven that electrospun scaffolds made from this recipe showed great structural stability and cytocompatibility[16,18,19]. Incorporation of synthetic polymers with natural polymers, such as gelatin greatly increases the surface hydrophilicity of the resulting electrospun scaffolds, which gives to the improved scaffold properties for cell adhesion and proliferation and enhances the cell-scaffolds interactions.

Mechanical properties of electrospun scaffolds are closely associated with their fiber anisotropic/isotropic characteristics[5,20]. Tensile strength along the prevailing fiber direction is much greater than the strength perpendicular to the fiber direction[13]. Both the aligned and yarn scaffolds showed evident fiber anisotropy along the predominant fiber direction, whereas the random scaffold exhibited isotropic fiber texture. With a focus on cell-secreted extracellular matrix products on the mechanical properties along the fiber direction of electrospun scaffolds, we measured the tensile strength parallel to the prevailing fiber direction accordingly. Our results showed that the aligned scaffold had a higher stress-strain curve[Fig.1(D)] with a significantly greater UTS[Fig.1(E)], a smaller strain rate[Fig.1(F)], and a much greater modulus[Fig.1(G)] than the random and yarn scaffolds. The random scaffold showed the greatest strain rate[Fig.1(F)], the smallest UTS[Fig.1(E)] and modulus[Fig.1(G)]. The yarn scaffold had intermediate tensile properties among the three scaffolds[Fig.1(D)—(G)]. These results indicated that the fiber density is also an important determiner of the mechanical properties of electrospun scaffolds.

3.2 Cell Growth on Electrospun Scaffolds

3.2.1 Cell Proliferation

Electrospun scaffolds mimic the nanofibrous microenvironment of the native extracellular matrix and have shown to be beneficial to cell proliferation[2]. NIH 3T3 fibroblast is a classical cell line that has been widely used to evaluate the cytocompatibility of electrospun scaffolds. CCK-8 assay indicated that murine fibroblasts steadily proliferated on these electrospun scaffolds with a significant increase in cell numbers over time(Fig.2). On days 1 and 4, there was no significant difference in cell proliferation rates among the three scaffolds, but the yarn scaffolds promoted greater proliferation of fibroblasts on day 7. This is in line with our previous reports that yarn scaffolds promoted proliferation rates of many cell lines including endothelial cells[12], pre-osteoblasts[12], and fibroblasts[13], as well as primary rabbit tendon cells[21]. In a recent report, we found that primary rabbit meniscus cells showed similar proliferation rates on yarn scaffolds compared with those on random scaffolds and aligned scaffolds[16]. This discrepancy is likely due to the inherently different proliferative capability of those cells. Cells can only proliferate on the surface of random and aligned scaffolds due to their dense nanofiber configuration and do not proliferate actively after confluence. In contrast, cells not only grow on the surface but also infiltrate into the inner of yarn scaffolds. In other words, cells experience a three-dimensional grow pattern within the yarn scaffolds. Rapid-proliferating cells, such as fibroblasts(Fig.2), endothelial cells, and tendon cells reach maximal numbers on the surface of random and aligned scaffolds, whereas these cells infiltrate into the inner of the yarn scaffold and continue to grow three-dimensionally and therefore exhibit greater proliferation rates[12,13,21]. For the slow-proliferating cells, they did not reach the maximum population on those scaffolds during the time course of investigation and therefore showed no significant difference in proliferation rate[16].

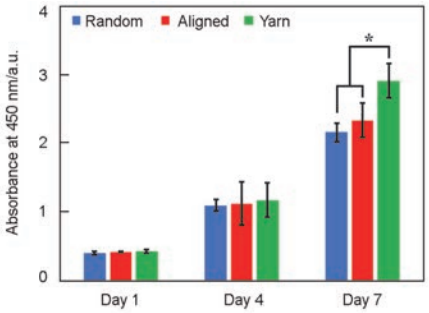

Fig.2 Proliferation rates of NIH 3T3 fibroblasts on electrospun scaffolds assessed by CCK-8 assay

Fibroblasts proliferate progressively over time. There is no significant difference in the proliferation rate of fibroblasts among three scaffolds from day 1 to day 4, while the yarn scaffold shows a significantly greater proliferation rate than the random and aligned scaffolds at day 7(p<0.05). n=4, two-way ANOVA followed by Tukey's post hoc test.

3.2.2 Cell Viability

Cell viability on these electrospun scaffolds was evaluated by live/dead staining(Fig.3). NIH 3T3 fibroblasts were sparsely distributed on scaffold surfaces with predominant live cells and a few dead cells on day 1[Fig.3(A)—(C)]. A huge increase

https://doi.org/10.1007/s40242-021-1024-7

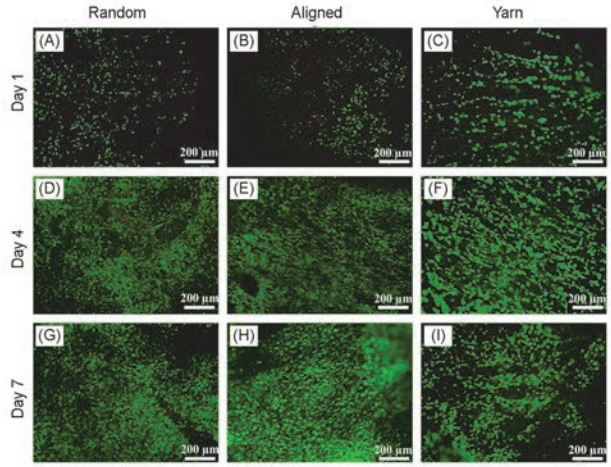

Fig.3 Live/dead staining of NIH 3T3 fibroblasts on electrospun scaffolds

Fibroblasts show good viability on scaffolds, on which they are predominately alive(green) with a small portion of dead cells(red). Fibroblasts proliferate well and show a great increase in cell numbers over time. (A)—(C) Day 1; (D)—(F) day 4; (G)—(I) day 7; (A), (D) and (G) random; (B), (E) and (H) aligned; (C), (F) and (I) yarn.

in live cell populations that almost fully cover the scaffold surface without an increase in dead cells on these electrospun scaffolds was observed thereafter from day 4[Fig.3(D)—(F)] to day 7[Fig.3(G)—(I)]. This result indicates great cytocompatibility of electrospun scaffold, regardless of their fibrous configuration. Live/dead staining also revealed distinct cell organizations on these scaffolds. Specifically, fibroblasts presented no cell orientation on the random scaffold[Fig.3(A), (D) and (G)]. Fiber alignment of the aligned and yarn scaffold guided the similar organization of aligned cells along with the fiber direction. Organized fibroblasts were confluent on the aligned scaffold[Fig.3(H)] without any empty space, while cells showed organized patterns covering yarns and left evident grooves between yarns on the yarn scaffold on day 7 [Fig.3(I)].

3.2.3 Cell Morphology

SEM images provide close views of cell-scaffold contact of NIH 3T3 fibroblasts on electrospun scaffolds(Fig.4). Fibroblasts showed polygonal shape on the random scaffold [Fig.4(A)], while they presented elongated morphology with cell orientation along the fiber direction on the aligned[Fig.4(B)] and yarn[Fig.4(C)] scaffolds on day 1. Afterward, fibroblasts showed increased coverage on the surfaces of scaffolds on day 4[Fig.4(D)—(F)] and completely covered scaffold surfaces on day 7[Fig.4(G)—(I)]. Interestingly, a few cells infiltrated into the inner part of the yarn scaffold through its rough grooves on day 4[Fig.4(F)], indicating that cells experience three-dimensional growth within the yarn scaffold. After 7 days, NIH 3T3 proliferating fibroblasts filled the grooves between

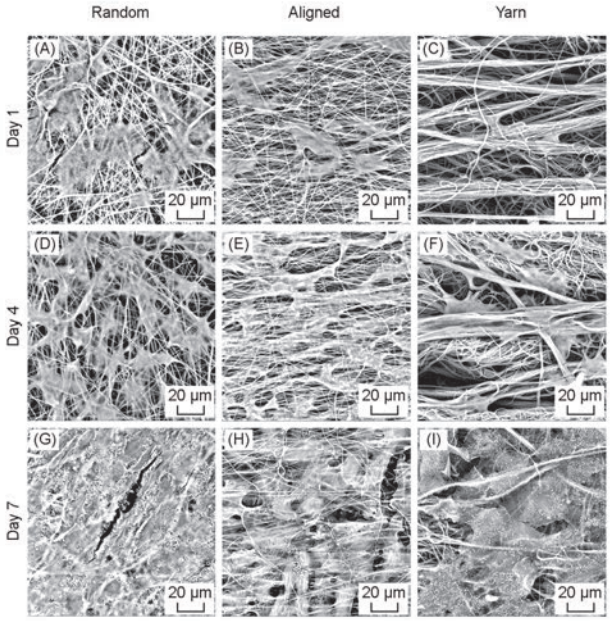

Fig.4 SEM images of NIH 3T3 fibroblasts on electrospun scaffolds

Fibroblasts exhibit polygonal shape on the random scaffolds and increase from day 1(A) to day 4(D) and then confluent on day 7(G). In contrast, fibroblasts are stretched along the fiber direction on the aligned(B, E, and H) and yarn(C, F, and I) scaffolds. (A)—(C) Day 1; (D)—(F) day 4; (G)—(I) day 7; (A), (D) and (G) random; (B), (E) and (H) aligned; (C), (F) and (I) yarn.

adjacent yarns. Although the absence of section views of cell-seeded yarn scaffolds to show cell infiltration in the current study, our previous studies have demonstrated extensive cell infiltration into yarn scaffolds[12,13,16,21]. These results demonstrate electrospun yarn scaffolds can be an excellent candidate for 3D cell growth, which recapitulate the microenvironment of the native extracellular matrix.

3.3 Cell-scaffold Interactions

3.3.1 Biomechanics of Cell-seeded Scaffolds

Biodegradable scaffolds degrade gradually by hydrolysis and enzymatic degradation when cultured with cells *in vitro*. Along with degradation, scaffolds show decreasing mechanical strength until complete degradation. Fibroblasts are known to produce extracellular matrix products that account for structural and mechanical support, which compensate for the mechanical loss due to scaffold degradation. In the current study, we found that NIH 3T3 fibroblasts did pose promotive effects on electrospun scaffolds to some extent(Fig.5). Specifically, cell-seeded scaffolds showed slightly higher UTS[Fig.5(A)—(C)] than the cell-free scaffolds, while no significant difference was observed(p=0.33 for random; p=0.09 for aligned; p=0.06 for yarn; two-way ANOVA). Fibroblasts showed little effect on the breaking strain rates of scaffolds that cell-seeded scaffolds had similar strain rates to their

https://doi.org/10.1007/s40242-021-1024-7

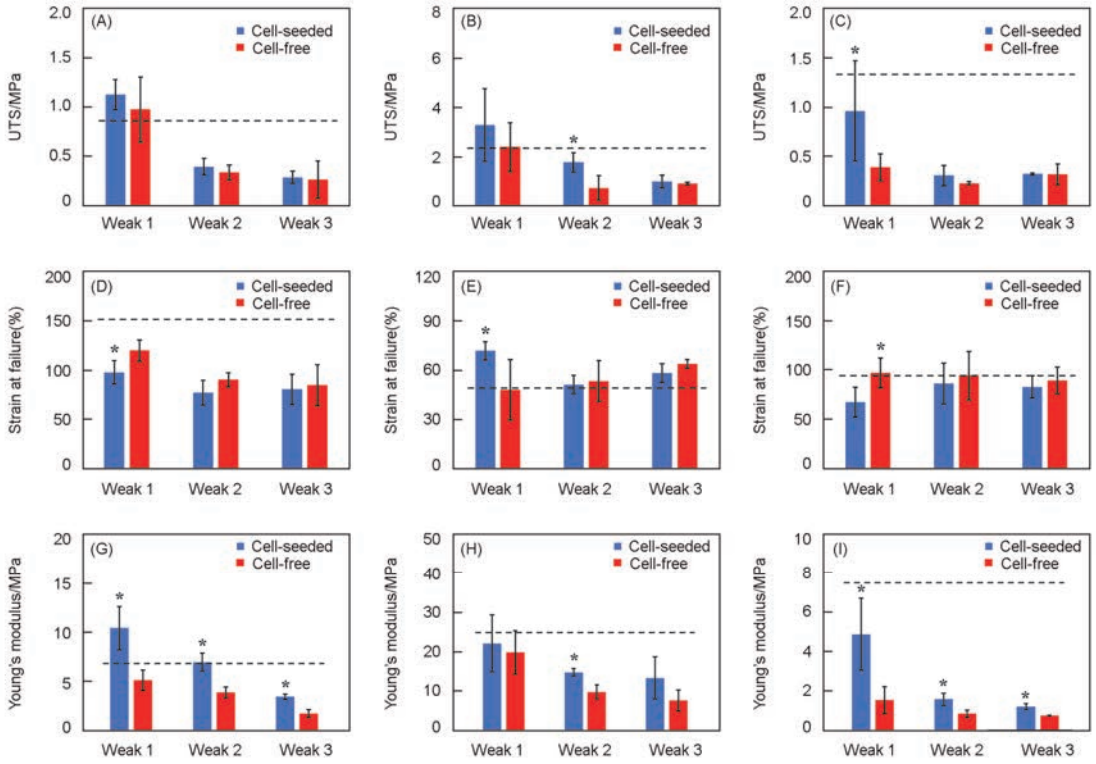

Fig.5 Uniaxial tensile properties of fibroblast-seeded electrospun scaffolds

(A), (D) and (G) Random; (B), (E) and (H) aligned; (C), (F) and (I) yarn. NIH 3T3 fibroblasts show negligible effects on the UTS(A—C) and strain at failure(D—F) of the three electrospun scaffolds. Fibroblasts significantly improve the tensile moduli of random(G) and yarn(I) scaffolds, whereas they do not promote Young's modulus of the aligned scaffold(H). Note: dashed lines indicate the values of UTS, strain at failure, and modulus of scaffolds read from Fig.1(E)—(G); n=4, two-way ANOVA with unpaired Student's t-test for comparing cell-seeded and cell-free scaffolds, * indicates p<0.05.

corresponding cell-free scaffolds during 3 weeks *in vitro* culture[Fig.5(D)—(F)]. In contrast, fibroblasts showed prominent effects on the tensile moduli of electrospun scaffolds[Fig.5(G)—(I)]. Cell-seeded random[Fig.5(G)] and yarn[Fig.5(I)] scaffolds exhibited significantly greater moduli than their corresponding cell-free controls at each time point(p<0.0001 for random; p=0.001 for aligned; two-way ANOVA). However, there is no significant difference between cell-seeded and cell-free scaffolds for the aligned scaffold[Fig.5(H)] during 3 weeks *in vitro* culture(p=0.07; two-way ANOVA). This result is in line with our previous study that rabbit meniscus cell-seeded aligned scaffolds showed comparable modulus with cell-free control, while meniscus cells promoted moduli of random and yarn scaffolds after 3 weeks[16]. It should be noted that, although there is no significant difference, we cannot rule out the contribution of fibroblasts to the modulus of the aligned scaffold. Cell-free random and yarn scaffolds showed a greater loss in modulus during the first week, which gave to 3—5 MPa difference compared with their corresponding cell-seeded scaffolds. The difference narrowed to 1—2 MPa and even less over time. This result indicates that the contribution of fibroblasts to the scaffold modulus can be 1—5 MPa, which is estimated to approximately 50% magnitude of that of cell-free scaffolds at each time point. Because the aligned scaffold had a relatively higher modulus, fibroblast contribution only accounts for 10% magnitude of that of cell-free scaffolds at each time point. Fibroblast contribution to aligned scaffolds might be overridden by the greater decrease in modulus of aligned scaffolds and by tolerated experimental error.

Some implications regarding the mechanical properties of cell-seeded electrospun scaffolds are worthy of discussion. We found the significance in terms of Young's modulus for the random and yarn scaffolds as early as 1 week post cell seeding, though the scaffolds were seeded with NIH 3T3 fibroblasts at a low density of 2×10^4 cells/cm^2. This is attributable to the rapid proliferation of NIH 3T3 fibroblasts shown by confluent cell layers on the scaffold surface(Fig.3 and 4). In future studies to investigate fibrotic diseases using primary cells with relatively slow proliferation rates, *e.g.*, cardiac fibroblasts[22,23] and lung fibroblasts[24], it is better to seed those scaffolds with cells at a higher density. As for the cell seeding matrix to dissect cell-scaffold interactions, it is critical for the scaffolds to have a biomimetic structure to simulate that of the native extracellular matrix. Considering the specific application of modeling cardiac fibrotic milieu that cardiac fibroblasts reside within a highly oriented extracellular matrix in a three-dimensional space, the yarn scaffold with a unique

https://doi.org/10.1007/s40242-021-1024-7

ultrastructure could be a better choice.

3.3.2 Collagen and Total Protein Deposition

Collagen is the major structural protein and under dynamic turnover in the body. Fibroblasts are the major cells producing collagen[8,25]. We quantified the NIH 3T3 fibroblast secreted collagen by hydroxyproline assay(Fig.6). Fibroblasts showed significantly increased collagen deposition on the three electrospun scaffolds from week 1 to week 3(p<0.0001, two-way ANOVA). Among those, the yarn scaffold promoted much greater collagen deposition than the other two scaffolds at week 2(p<0.05, two-way ANOVA), and the difference in collagen deposition became greater at week 3(p<0.01, two-way ANOVA). The increased collagen deposition could be attributed to the greater capacity of the yarn scaffold in supporting cell growth that fibroblasts experience three-dimensional growth within the yarn scaffold and reach a greater population(Fig.2). It is therefore not surprising that the yarn scaffold had greater collagen deposition due to its increased and significantly greater population of fibroblasts[16]. Another factor contributing to the elevated collagen deposition might be associated with the unique fiber configuration, in which fibroblasts reside and reciprocally interact with their surrounding three-dimensional microenvironment. In this scenario, fibroblasts-secreted collagen was attached to the yarns and nanofibers throughout the whole scaffold in a three-dimensional manner. In contrast, collagen was only deposited on the surfaces of random and aligned scaffolds. This result indicates that the yarn scaffold provides a suitable nanofiber matrix structure for fibroblast growth and extracellular matrix deposition, and could be a better choice for modeling fibrotic disorders *in vitro* than conventional two-dimensional platforms[22,26]. Further studies should investigate the presence and differentiate the type of collagen of the yarn scaffold *via* immunofluorescence imaging[27,28]. Besides, external stimuli, such as growth factors[29,30] and mechanical stretching[31,32] might be involved in yarn scaffold-based fibrotic models to drug screening[33].

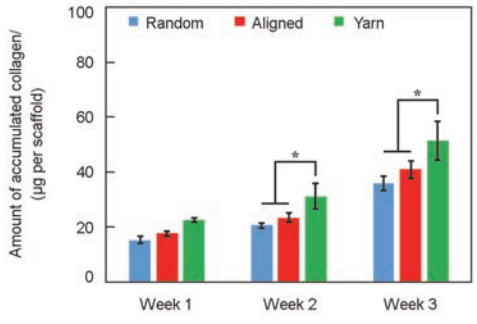

Fig.6 Collagen accumulation quantified by hydroxyproline assay

Electrospun scaffolds show significantly increased accumulation of collagen over 3 weeks(p<0.05). NIH 3T3 fibroblasts generate significantly greater collagen than the random and aligned scaffolds at week 2 and week 3(p<0.05). n=4, two-way ANOVA followed by Tukey's post hoc test.

Total protein deposition of NIH 3T3 fibroblasts on electrospun scaffolds was determined by BCA assay(Fig.7). Although electrospun scaffolds allowed significantly increased amounts of total protein over time(p<0.005, two-way ANOVA), there is no significant difference among those scaffolds at each time point(p>0.05, two-way ANOVA). At each time point, the total protein(Fig.7) was approximately 10 folds that of the collagen(Fig.6) on each scaffold, which is in line with our recent study on rabbit meniscus cell producing protein and collagen[16]. These results suggest that fibroblasts might produce collagen in a more sensitive way to the cultured matrix than that they produce total protein. In other words, the yarn scaffold poses more profound effects on fibroblasts to generates collagen than their capability to produce total protein. Collagen is the predominant interest of extracellular matrix products of fibrotic disorders[34,35], it is better to select the deposition of collagen rather than total protein as a determinant when utilizing the yarn scaffolds for cardiac fibrotic modeling.

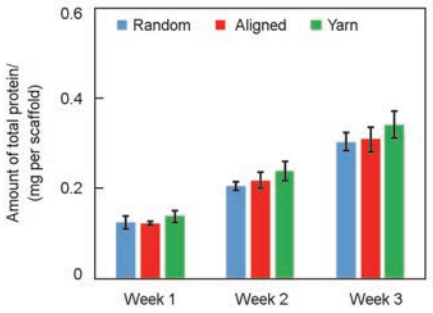

Fig.7 Total protein accumulation quantified by BCA assay

The three electrospun scaffolds support progressively increased accumulation of total protein over 3 weeks. There is no significant difference in total protein accumulation among those scaffolds at each time point(p>0.05). n=5, two-way ANOVA followed by Tukey's post hoc test.

4 Conclusions

Electrospun scaffolds with distinct fiber configurations directed different cell growth patterns and showed various interplays with fibroblasts. The yarn scaffold supported three-dimensional cell growth with a greater proliferation rate than electrospun random and aligned scaffolds. Cell-seeded yarn scaffolds exhibited greater tensile strength and Young's modulus than cell-free scaffolds. Taken together with its porous aligned nanofiber configuration, the electrospun yarn scaffold potentiates to be matrix materials for modeling cardiac fibrosis *in vitro*.

https://doi.org/10.1007/s40242-021-1024-7

Acknowledgements

This work was supported by the Fund of Donghua University, China (No.2232019D3-20), the Fund of the Science and Technology Commission of Shanghai Municipality, China(No.19440741300) and the National Natural Science Foundation of China(No.31900949).

Conflicts of Interest

The authors declare no conflicts of interest.

References

[1] Zhu T., Gu H., Zhang H., Wang H., Xia H., Mo X., Wu J., *Acta Biomater*., **2021**, *119*, 211
[2] Dziemidowicz K., Sang Q., Wu J., Zhang Z., Zhou F., Lagaron J. M., Mo X., Parker G. J. M., Yu D.-G., Zhu L.-M., Williams G. R., *J. Mater. Chem. B*, **2021**, *9*, 939
[3] Wu T., Mo X., Xia Y., *Adv. Healthcare Mater*., **2020**, 9, 1901761
[4] Lin W., Chen M., Qu T., Li J., Man Y., *J. Biomed. Mater. Res. B Appl. Biomater*., **2020**, *108*, 1311
[5] Yeo M., Kim G., *Acta Biomater.*, **2020**, *107*, 102
[6] Chen H., Lui Y. S., Tan Z. W., Lee J. Y. H., Tan N. S., Tan L. P., *Adv. Healthcare Mater*., **2019**, *8*, 1801378
[7] Abou Neel E. A., Bozec L., Knowles J. C., Syed O., Mudera V., Day R., Hyun J. K., *Adv. Drug Del. Rev*., **2013**, *65*, 429
[8] DeLeon-Pennell K. Y., Barker T. H., Lindsey M. L., *Matrix Biol*., **2020**, *91/92*, 1
[9] Humeres C., Frangogiannis N. G., *JACC Basic Transl. Sci*., **2019**, *4*, 449
[10] Jin J., Togo S., Kadoya K., Tulafu M., Namba Y., Iwai M., Watanabe J., Nagahama K., Okabe T., Hidayat M., Kodama Y., Kitamura H., Ogura T., Kitamura N., Ikeo K., Sasaki S., Tominaga S., Takahashi K., *Respir. Res*., **2019**, *20*, 119
[11] Sacchi M., Bansal R., Rouwkema J., *Trends Biotechnol*., **2020**, *6*, 623
[12] Wu J., Huang C., Liu W., Yin A., Chen W., He C., Wang H., Liu S., Fan C., Bowlin G. L., Mo X., *J. Biomed. Nanotechnol.*, **2014**, *10*, 603
[13] Wu J., Liu S., He L., Wang H., He C., Fan C., Mo X., *Mater. Lett.*, **2012**, *89*, 146
[14] Wu T., Zheng H., Chen J., Wang Y., Sun B., Morsi Y., El-Hamshary H., Al-Deyab S. S., Chen C., Mo X., *J. Mater. Chem. B*, **2017**, *5*, 139
[15] Zhang K., Cao N., Guo X., Zou Q., Zhou S., Yang R., Zhao W., Mo X., Liu W., Fu Q., *Neurourol. Urodyn*., **2018**, *37*, 978
[16] Wang X., Zhu J., Sun B., Jin Q., Li H., Xia C., Wang H., Mo X., Wu J., *J. Biomed. Mater. Res. B Appl. Biomater*., **2021**, *109*, 201
[17] Liu X., He X., Jin D., Wu S., Wang H., Yin M., Aldalbahi A., El-Newehy M., Mo X., Wu J., *Acta Biomater*., **2020**, *108*, 207
[18] Molina E. R., Chim L. K., Salazar M. C., Mehta S. M., Menegaz B. A., Lamhamedi-Cherradi S.-E., Satish T., Mohiuddin S., McCall D., Zaske A. M., Cuglievan B., Lazar A. J., Scott D. W., Grande-Allen J. K., Ludwig J. A., Mikos A. G., *Acta Biomater*., **2019**, *100*, 38
[19] Feng B., Wang S., Hu D., Fu W., Wu J., Hong H., Domian I. J., Li F., Liu J., *Acta Biomater*., **2019**, *83*, 211
[20] Jia Y., Yang W., Zhang K., Qiu S., Xu J., Wang C., Chai Y., *Acta Biomater*., **2019**, *83*, 291
[21] Xu Y., Wu J., Wang H., Li H., Di N., Song L., Li S., Li D., Xiang Y., Liu W., Mo X., Zhou Q., *Tissue Eng. Part C: Methods*, **2013**, *19*, 925
[22] Kong M., Lee J., Yazdi I. K., Miri A. K., Lin Y.-D., Seo J., Zhang Y. S., Khademhosseini A., Shin S. R., *Adv. Healthc. Mater*., **2019**, *8*, 1801146
[23] Huang S., Chen B., Su Y., Alex L., Humeres C., Shinde A. V., Conway S. J., Frangogiannis N. G., *J. Mol. Cell. Cardiol*., **2019**, *132*, 84
[24] Ng-Blichfeldt J.-P., Jong T. D., Kortekaas R. K., Wu X., Lindner M., Guryev V., Hiemstra P. S., Stolk J., Königshoff M., Gosens R., *Am. J. Physiol. Lung Cell Mol. Physiol*., **2019**, *317*, L14
[25] Daseke M. J., Tenkorang M. A. A., Chalise U., Konfrst S. R., Lindsey M. L., *Matrix Biol.*, **2020**, *91/92*, 109
[26] Deddens J. C., Sadeghi A. H., Hjortnaes J., van Laake L. W., Buijsrogge M., Doevendans P. A., Khademhosseini A., Sluijter J. P., *Adv. Healthcare Mater*., **2017**, *6*, 1600571
[27] Tao Z.-W., Wu S., Cosgriff-Hernandez E. M., Jacot J. G., *Acta Biomater.*, **2020**, *101*, 206
[28] Huang K., Ozpinar E. W., Su T., Tang J., Shen D., Qiao L., Hu S., Li Z., Liang H., Mathews K., Scharf V., Freytes D. O., Cheng K., *Sci. Transl. Med*., **2020**, *12*, 538
[29] Vainio L. E., Szabó Z., Lin R., Ulvila J., Yrjölä R., Alakoski T., Piuhola J., Koch W. J., Ruskoaho H., Fouse S. D., Seeley T. W., Gao E., Signore P., Lipson K. E., Magga J., Kerkelä R., *JACC Basic Transl. Sci*., **2019**, *4*, 83
[30] Fix C., Carver-Molina A., Chakrabarti M., Azhar M., Carver W., *J. Cell. Physiol*., **2019**, *234*, 13931
[31] Asmani M., Velumani S., Li Y., Wawrzyniak N., Hsia I., Chen Z., Hinz B., Zhao R., *Nat. Commun*., **2018**, *9*, 2066
[32] Yong K. W., Li Y., Huang G., Lu T. J., Safwani W. K., Pingguan-Murphy B., Xu F., *Am. J. Physiol. Heart Circ. Physiol*., **2015**, *309*, H532
[33] Savoji H., Mohammadi M. H., Rafatian N., Toroghi M. K., Wang E. Y., Zhao Y., Korolj A., Ahadian S., Radisic M., *Biomaterials*, **2019**, *198*, 3
[34] Henderson N. C., Rieder F., Wynn T. A., *Nature*, **2020**, *587*, 555
[35] Karsdal M. A., Nielsen S. H., Leeming D. J., Langholm L. L., Nielsen M. J., Manon-Jensen T., Siebuhr A., Gudmann N. S., Rønnow S., Sand J. M., Daniels S. J., Mortensen J. H., Schuppan D., *Adv. Drug Del. Rev*., **2017**, *121*, 43